Resistive Interchange Mode destabilized by Helically Trapped Energetic Ions and its Effects on Energetic Ions and Bulk Plasmas

X.D. Du[1], K. Toi, M. Osakabe, S. Ohdachi, T. Ido, K.Tanaka, M. Yokoyama, M.Yoshinuma, K. Ogawa, M. Isobe, K. Nagaoka, T. Ozaki, S. Sakakibara, R. Seki, Y.Suzuki, K.Y. Watanabe and LHD Experiment Group

[1]The Graduate University for Advanced Study, Toki 509-5292, Japan
National Institute for Fusion Science, Toki 509-5292, Japan

E-mail contact of main author: du.xiaodi@lhd.nifs.ac.jp

Abstract: A resistive interchange mode with bursting behavior and rapid frequency chirping in the range less than 10 kHz is observed for the first time in the magnetic hill region of net current-free, low beta LHD (Large Helical Device) plasmas during high power injection of perpendicular neutral beams. The mode resonates with the precession motion of helically trapped energetic beam ions, following the resonant condition. The radial mode structure is found to be very similar to that of usual pressure-driven interchange mode, of which radial displacement eigenfunction has an even function around the mode rational surface. This beam driven mode is excited when the beta value of helically trapped energetic ions exceeds a certain threshold. The radial transport of helically trapped energetic ions induced by the mode transiently generates significant radial electric field near the plasma peripheral region. Thus generated radial electric field is thought to contribute to suppression of micro turbulence and transient improvement of bulk plasma confinement, suggesting strong flow shear generation.

1. Introduction

The resistive interchange mode (RIC) is destabilized by finite pressure gradient in magnetic hill and it can be excited even below the beta limit predicted by the Mercier criterion when the magnetic shear stabilization effect disappears due to the effect of resistivity [1]. In recent years, RIC is studied experimentally for H-mode plasmas with steep pressure gradient near the edge in the Large Helical Device (LHD) [2-3], since the magnetic hill exists in the peripheral region [4]. It's found that the RICs localize at the mode rational surface having an even function structure with fairly narrow width [5-8]. According to linear MHD theory, the growth rate of RIC is predicted as $\gamma_{RIC} \propto L_p^{-2/3} g^{2/3} \eta^{1/3} L_s^{2/3}$ [9], where L_p, g, η and L_s are the scale length of pressure gradient, the averaged magnetic curvature, electrical resistivity and the magnetic shear length at the rational surface respectively. From these facts, the fluctuation amplitude is inferred to increase with plasma beta value β and decrease with magnetic Reynolds number S [10]. Experimental results in LHD support the prediction [11].

Recently, a strong bursting mode, excited by the injection of perpendicular hydrogen beamlines (PERP-NBI), has been observed in the low frequency range ($f < 10kHz$) with rapid frequency chirping in net current-free, low β plasmas ($\beta < 1\%$) of LHD. The mode having $m = 1/n = 1$ localizes at the $\iota/2\pi = 1$ flux surface with a similar displacement eigenfunction of RIC, where m and n are poloidal and toroidal mode numbers, respectively. In this region, the helical field ripple is large, i.e., ε_h~0.15. Consequently, energetic ions generated by PERP-NBI are deeply trapped in the helical ripple, and are called 'helically trapped energetic ions' [12]. The helically trapped energetic ions can go around the torus having precession motions toroidally and poloidally, along the helical valley of magnetic field strength. It is important that the precession frequency is close to the observed frequency of the bursting mode. The initial frequency of the bursting mode having rapid frequency chirping agrees well with the resonance frequency predicted by the resonance condition between the MHD modes and helically trapped energetic ions in LHD magnetic configuration. The resonance condition is determined by various Fourier components of the magnetic field

spectrum of a helical device such as LHD. In this paper, the characteristics of the bursting modes and the effects on energetic ion confinement are discussed. The impacts on bulk plasma are also discussed. Hereafter, we call helically trapped **E**nergetic ions driven resistive **I**nter**C**hange mode as EIC.

2. Observation of EIC mode

To understand the excitation mechanism of EIC, an experiment is conducted to destabilize EIC by only PERP-NBI of beam energy $E_b = 34keV$, based on the consideration that the characteristic frequency of passing particles such as transit frequency, produced by high energy tangential NBI of $E_b = 180keV$, is much higher than the observed mode frequency less than $\sim 10kHz$. In this experiment, electron cyclotron heating (ECH) with 77GHz is employed to maintain the plasma performance throughout the discharge. A full modulated beamline of PERP-NBI of $\sim 1.8MW$ deposition power is injected throughout the discharge and the other beamline of $\sim 1.8MW$ is superimposed during the short time window from $4.0s$ to $4.18s$, as shown in Fig. 1(d). An oscillatory mode destabilized weakly is observed in magnetic probes just after the second beamline is superimposed, as shown in Figs. 1(a) and (b). The destabilization of the oscillatory mode, which is thought to be RIC, is caused by the increase of total plasma beta including bulk plasma and beam ions by PERP-NBI. In the latter half of the superimposed PERP-NBI phase from $t = 4.1s$ to 4.18s, strong bursting events are detected in magnetic probes. From the expanded view shown in Fig. 1(a), the oscillatory mode of $\sim 2kHz$ is firstly destabilized. Then, the magnetic fluctuation amplitude is suddenly enhanced with strongly distorted waveforms instead of sinusoidal oscillations. An important point is that the mode frequency suddenly jumps up to $\sim 8kHz$, and then rapidly chirps down to $\sim 2kHz$ in $\sim 2ms$, exhibiting the characteristics of EP-driven fishbone like instabilities. Finally, the amplitudes of oscillatory modes are considerably reduced for a short time period of $\sim 5ms$ after each burst. The Doppler frequency evaluated from the carbon toroidal flow measurement by charge exchange recombination spectroscopy (CXRS) [13], is significantly small, compared with the mode frequency $f_{doppler} \ll f_{EIC}$, because the non-axisymmetric magnetic field structure brings about large parallel viscosity and strongly slows down the toroidal flow in plasma peripheral region of LHD, in particular, on the condition without the momentum input from tangential NBI. In

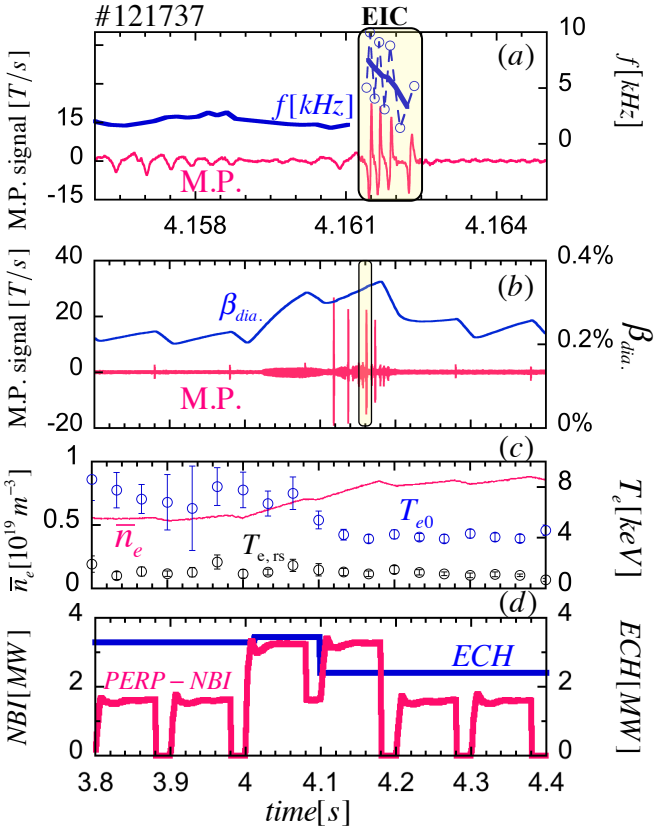

Fig. 1 Time evolution of a plasma heated by PERP-NBI and ECH where the toroidal field is $B_t = 2.75T$ and the magnetic axis position of the vacuum field is $R_{ax} = 3.6m$. The expanded view of magnetic probe (M.P.) signal (red) and its frequency (blue) (a), the time evolution of M.P. signal (red) and diamagnetic beta (blue) (b), electron temperature measured at center (blue) and mode rational surface (black) and line averaged electron density measured by FIR (red) (c), deposited ECH (blue) and PERP-NBI (red) power (d).

the low power phase of PERP-NBI after $t = 4.18s$, the bursting mode is no longer destabilized as seen from Fig. 1. It suggests that EIC can only be destabilized by large amount of helically trapped energetic ions produced with intense PERP-NBI. According to the phase analysis of magnetic probe array, both oscillatory and bursting modes with $m = 1/n = 1$ structure propagate in the electron diamagnetic drift direction poloidally and counter-B_t direction toroidally in plasma frame. This is typical propagation direction of RIC observed in plasma frame in LHD.

3. Orbits of helically trapped energetic ions and resonant condition

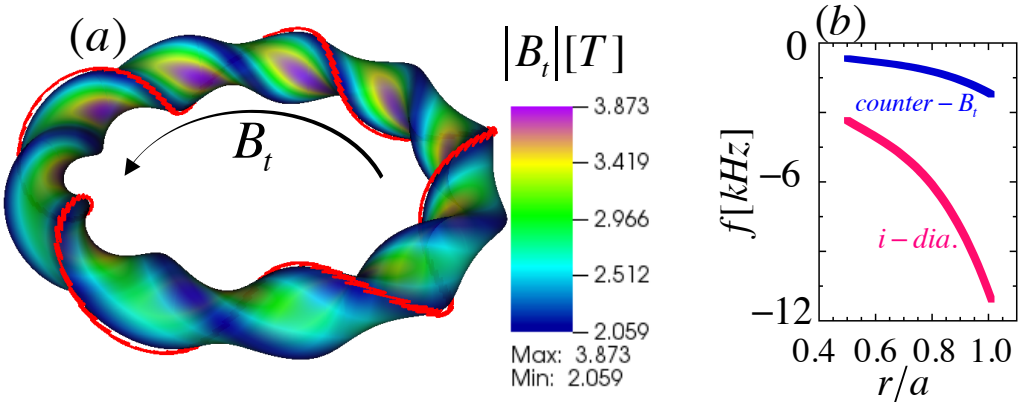

Fig. 2 (a) The contour plot of the magnetic field strength and the calculated orbit of helically trapped protons (red). (b) The calculated poloidal (red) and toroidal (blue) precession frequencies.

To investigate the resonance between EIC and energetic ions, the orbit of helically trapped energetic ions produced by PERP-NBI is investigated numerically by a full orbit code called 'LORBIT' [14]. One typical example is depicted in Fig. 2(a). A proton with energy $E_b = 34keV$ and pitch angle $\chi = 85°$ is launched from the $\iota/2\pi = 1$ flux surface and tracked numerically. It can be seen that the proton makes a bounce motion and is deeply trapped in the helical ripple well. Simultaneously, it also slowly circulates helically around the torus with the helical pattern $\cos(l\theta + N\phi)$ in the ion diamagnetic drift direction poloidally and in the counter-B_t direction toroidally, being trapped in the magnetic valley where the magnetic field is weak ($l = 2$: polarity of helical field, $N = 10$: toroidal field number). Note that there are two magnetic valleys existing in LHD due to the existence of a pair of helical coils. The toroidal and poloidal precession frequency of helically trapped ions are calculated in the flux coordinate. The result is shown in Fig. 2(b). From the calculation results, the absolute value of the poloidal precession frequency increases radially from $3kHz$ at $r/a \sim 0.5$ to $12kHz$ at the plasma boundary, where the negative sign of the precession frequencies stand for the ion diamagnetic drift direction poloidally and counter toroidal field direction toroidally. The toroidal precession frequency is found to be $f_{tor}^{prec} = (l/N) f_{pol}^{prec}$, as expected, due to the topology of the helical coils. The resonant condition for a helical plasma is given by [15]

$$f_{MHD} - (m + j\mu)\langle f_{pol}^{prec} \rangle + (n + j\nu N)\langle f_{tor}^{prec} \rangle = 0 \qquad (1)$$

where $j = 0, \pm 1$. Here, the precession motions in the magnetic field structure are expressed by the Fourier components $[\mu, \nu]$. The resonant frequencies for EIC are calculated by substituting the precession frequency of the helically trapped energetic ions at the mode rational surface. The observed frequency of EIC is consistent with the calculated frequency

corresponding to the bumpiness component [0,1] of the precession motion with $j=+1$, that is, $f_{MHD}=-1.2f_{\theta}^{prec.}=8.4kHz$. It indicates that the EIC can resonate with the precession motion of helically trapped energetic ions, even if EIC propagates poloidally in the opposite direction to that of the energetic ions.

4. Mode Structures

The mode structures of RIC and EIC are derived from the fluctuations of Soft X-ray (SX) emission [16]. Radial displacement induced by interchange mode can be modeled as a Gaussian shape [5-7],

$$\xi_r(r)=A_0\cdot\exp\left\{-\left[\left(\rho-\rho_{peak}\right)/\Delta_w\right]^2\right\}\cos(m\theta-\omega t) \qquad (2)$$

Here ξ_r is the plasma displacement, A_0 is the amplitude, Δ_w is the width of the mode structure, normalized by the minor plasma radius. The position of the mode peak ρ_{peak} corresponds to the mode rational surface. The plasma displacement is integrated spatially and temporally along the sightlines of the SX system so that the calculated profiles of the amplitude and phase as function of major radius should best-fit to the observed profiles of SX data by adjusting the above parameters of eq. (2). For both RIC and EIC having $m=1$, the best-fitting is obtained with the same parameters $\rho_{peak}=0.85$ and $\Delta_w=0.1$ with different mode amplitude A_0, and the both eigenfunctions have a quite similar shape. The phase of plasma displacement remains the same across the mode rational surface, suggesting an interchange-type mode instead of the tearing-type one. Additionally, the radial displacement of EIC is also derived from the data of electron cyclotron emission (ECE) diagnostic [17], as $\delta T_e/|\nabla T_e|$ (δT_e : electron temperature fluctuation, ∇T_e : the gradient of equilibrium electron temperature). This agrees well with the best-fitted mode structure derived from SX system. It is concluded that the mode has an interchange-type structure and localizes at the mode rational surface with a narrow mode width.

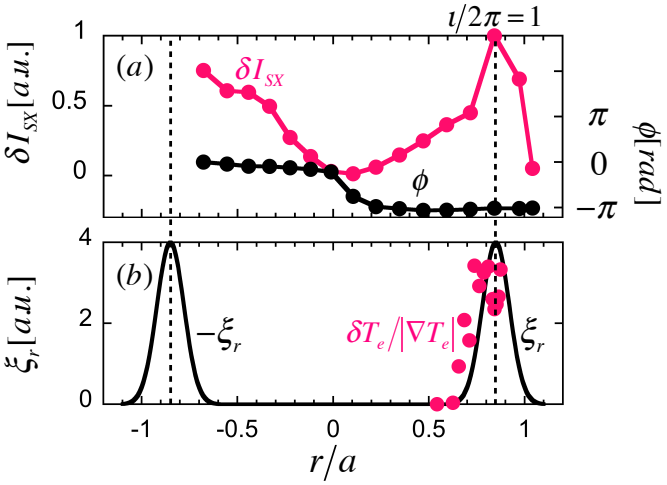

Fig. 3 (a) The fluctuation of SX emission for EIC (red) and the phase difference between each channel (black). (b) The ratio of temperature fluctuation and temperature gradient measured by ECE for EIC (dot) and the assumed plasma displacement to best fit the measured fluctuation of SX emission (line).

A sudden transition from RIC to EIC takes place when the beta of helically trapped beam ions β_{hot} reaches a certain threshold. In one specific experiment, RIC is firstly destabilized by the continuous increment of the bulk plasma beta from 0.61% to 0.65%. In this phase, electron temperature rises faster than the gradual decrease of electron density. With the further decrement of electron density with the constant power of PERP-NBI, EIC is observed with the jump of mode frequency. It suggests the existence of threshold of the energetic ion pressure P_{hot} or the beta value β_{hot} for the transition. The threshold of P_{hot} estimated from the PERP-NBI power deposition calculated by "FIT3D" code [18] is $P_{hot}/P_{bulk}\sim 20\%$.

5. Rapid change of energetic neutral flux

The impacts of EIC on the confinements of helically trapped ions are investigated by a compact neutral particle analyzer (CNPA) with fast time response of $0.1ms$ [19]. The sightlines of CNPA are arranged to monitor the neutral flux perpendicular to the magnetic field line and it can detect the energy distribution from the thermal ions of $\sim 0.8keV$ up to energetic ions of $\sim 150keV$. Typical contour plot of energetic neutral flux in a shot having EIC is shown in Fig. 4. The neutral flux suddenly increases in $E_b < 32keV$ synchronizing with each EIC burst. This indicates "clump" formation through resonant interaction between EIC and helically trapped energetic ions, as similar to the case of TAE bursts [20]. However, the "hole" is not clearly observed so far. The neutral flux detected by CNPA can be expressed as $\Gamma_0 = \int_V n_{EP} n_0 \langle \sigma v \rangle dV$, where n_{EP} and n_0 are the densities of the energetic ions and neutrals, respectively. The integration volume V is determined by the sightline and the solid angle of the detector of CNPA viewing an LHD plasma. The observed increase of energetic neutral flux in the range of $5 \sim 30keV$ is interpreted that the resonant energetic ions are transported by EIC from the mode rational surface area to the edge region of higher neutral density, because the reduction of H_α emission during EIC burst does not indicate the increased neutrals there. The energy range that neutral fluxes change rapidly is consistent with the resonant condition, which again suggests the resonant interaction of EIC and the helically trapped energetic ions of $E_b \sim 34keV$ produced by PERP-NBI.

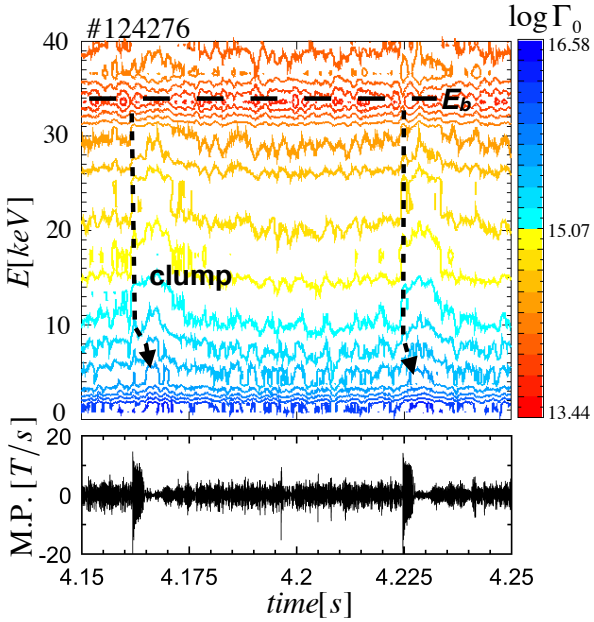

Fig. 4 The time evolution of contour plot of neutral flux from 0keV to 40keV (upper), and the two EICs in magnetic probe signal (lower).

6. Generation of negative radial electric field

It is interesting to measure the plasma potential change induced by EIC, since rapid radial transport of the helically trapped energetic ions in plasma peripheral region and non-ambipolarity of EP transport by EIC are expected. In this experiment, the heavy ion beam probe (HIBP) is employed to measure the plasma potential change by detecting the energy of secondary beam of Au^{2+} beam ions [21]. Figure 5 shows a significant and sharp reduction of plasma potential in plasma core region of $r/a \le 0.5$, corresponding to each EIC burst. The potential drop tends to increase and saturate with the increase of energetic neutral flux, as shown in Figs. 5(b) and (c). The observed large and sudden potential drop indicates that non-ambipolar radial transport of helically trapped fast ions is clearly induced by EICs. The radial profiles of the plasma potential drop induced by EICs having nearly same amplitude are obtained by a 10Hz radial sweep of a probe beam of HIBP in the magnetic configurations of $R_{ax} = 3.6m$ and $R_{ax} = 3.75m$, where the time duration of the EIC of $\sim 3ms$ is much smaller than the radial scanning period of the beam of $50ms$. In the $R_{ax} = 3.6m$ configuration, the beam can access the region of $0 < r/a < 0.6$ and the measured potential drop is about $13kV$

and uniform over the region. Note that, LHD plasma is surrounded by a stochastic region of magnetic field outside the last closed flux surface (LCFS) and the plasma potential is supposed to be positive outside the LCFS due to the rapid loss of electrons. That is, it is expected that a significant negative radial electric field would be generated by EIC in the plasma peripheral region of $0.6 < r/a < 1.0$. Moreover, in the $R_{ax} = 3.75m$ configuration, the probe beam can pass through the wider region of $0 < r/a < 0.9$, compared with that in the $R_{ax} = 3.6m$ configuration. The uniform potential drop of $13kV$ in the core and continuous increase of plasma potential over the region of $0.6 < r/a < 0.9$ clearly indicate generation of negative radial electric field there. To estimate the amplitude of this radial electric field induced by EIC, the profile of the radial electric field is modeled as $\Delta E_r = -85 \cdot \exp\left[-\left(\rho - 0.85/0.15\right)^2\right] kV/m$. The radial profile of the potential change derived by the radial integration of ΔE_r from LCFS toward the plasma center shows good agreement with the observed radial profile of potential drop.

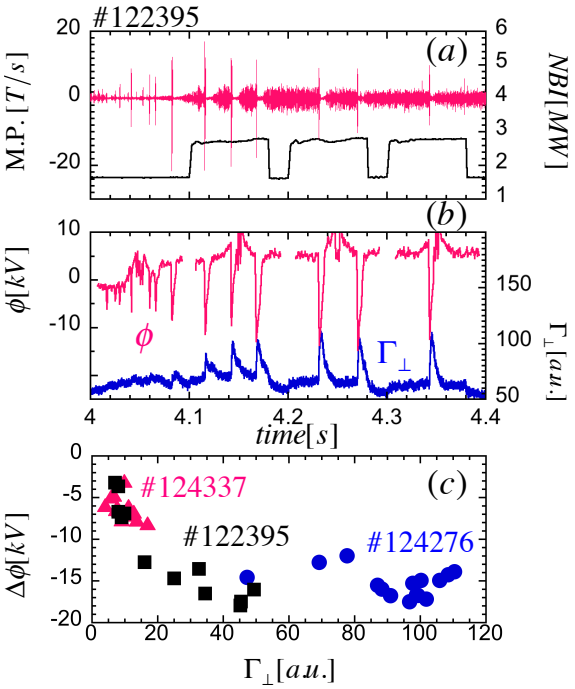

Fig. 5 The time evolution of magnetic probe signals (red) and the power of PERP-NBI (black) (a), the plasma potential in the core (red) and perpendicular energetic neutral flux of $E_0 > 10keV$ (blue) (b), the reduction of plasma potential in the core as the function of increment of perpendicular energetic neutral flux of $E_0 > 10keV$ in three shots (c).

7. Change of plasma flow by EIC

The HIBP data shows a significant radial electric field of $\sim 85\,kV/m$ near the edge is transiently formed by EIC. Thus, it is expected that generated radial electric field could induce or modify plasma mean flow and sheared flow. The change of plasma rotation induced by EIC is investigated by CXRS. The CXRS probes the Doppler effect on spectral lines of C^{6+} to acquire the mean velocity of thermal ions after a relaxation time between C^{6+} and proton, which is typically $\tau_{CH} \sim 10ms$. However, the typical time scale of EIC is $\tau_{EIC} \sim 3ms$ and the typical relaxation time between C^{6+} and C^{6+} is $\tau_{CC} \sim 0.5ms$. This means that the time evolution of plasma rotation detected by CXRS during EIC can only exhibit the temperature and flow change of the carbon impurity and does not necessarily reflect the change of bulk flow velocity of thermal fuel ions, even though the mean flow of thermal ions are also modified

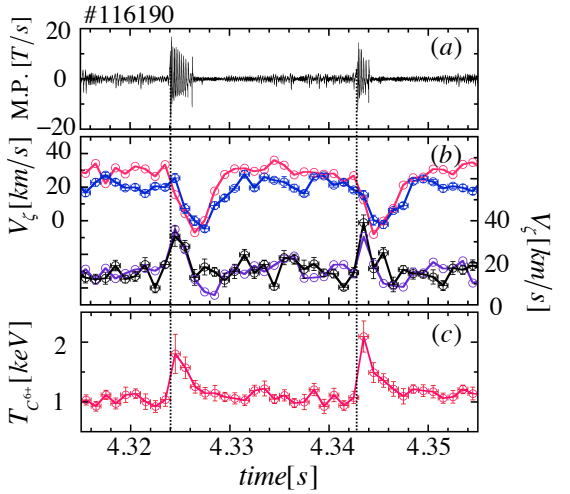

Fig. 6 The time evolution of two EICs in magnetic probe signal (a), plasma toroidal rotation at r/a~0.8 (red), r/a~0.85 (blue), r/a~0.92 (black) and r/a~0.98 (purple) (b), the carbon temperature around the mode rational surface (c).

by EIC. The result of toroidal rotation change of the carbon ion is shown in Fig. 6(b). It is enhanced in counter-B_t direction in the region of $0.3 < r/a < 0.9$ by each EIC. Interestingly, the toroidal rotation in the very edge region of $r/a > 0.9$ is enhanced in the opposite direction, that is, co-B_t direction.

The neoclassical theory of non-axisymmetric net-current-free toroidal plasma is employed to model the observed toroidal rotation change. Since the above-mentioned EIC-induced radial electric field is a dominant term for the small neoclassical electric field and the diamagnetic terms. Thus, the change of plasma toroidal flow of carbon impurity can be expressed as: $\vec{u}_{EIC} = (R/J)^2 \left(\langle G_{BS} \rangle_i / r \right) \phi'_{EIC}$, where $\vec{u}_{EIC}$ is the EIC-induced toroidal rotation change, $J \equiv RB_\phi$, and $\psi \equiv r^2 B_\phi / 2$. The quantity $\langle G_{BS} \rangle_i$ is the geometric factor [22]. In LHD magnetic configurations of $R_{ax} = 3.6m$ and $3.75m$, $\langle G_{BS} \rangle_i$ decreases toward the plasma edge, and finally changes the sign in the very edge region of $0.95 < r/a < 1.0$ [22, 23]. The toroidal rotation change calculated by the above equation using the HIBP data shows good agreement with the measured toroidal flow change by CXRS, including the flow reversal in the plasma peripheral region.

8. Suppression of density fluctuation

In LHD, the edge plasma transport is supposed to be dominated by turbulent transport. The effects of EIC on density fluctuations related to micro-turbulence are studied with the 2D Phase Contract Imaging diagnostic system (PCI) [24]. Density fluctuations in the frequency range of $20kHz$ to $500kHz$ are measured by this technique in the region of $0.3 < r/a < 1.0$. Intense density fluctuations propagating in the ion-diamagnetic drift direction in plasma frame are clearly identified around the phase velocity of $5\,km/s$, as the parts are encircled with rectangular frames in Fig. 7(a). On the other hand, the density fluctuations are significantly suppressed during an EIC burst. The suppressed density fluctuations have a peak around the perpendicular wavenumber normalized by thermal ion gyro radius $k\rho_{T_i} \sim 0.3$ at $r/a \sim 0.85$. It should be noted that the density fluctuation components are appreciably enhanced in the electron diamagnetic drift direction in both inboard and outboard sides, as seen from Fig. 7(b). An electrostatic gyrokinetic linear stability calculation is carried out with the GS2 code [25], including multiple species, fully kinetic descriptions of all species and collision, to infer the candidate electrostatic fluctuations [26]. The result suggests that the suppressed turbulence is likely to be ion temperature gradient (ITG) mode [26], as well as in the previous study [27], which locates in the region of $0.5 < r/a < 1.0$ with a peak at $r/a \sim 0.8$ and propagates in the ion diamagnetic drift direction. The linear growth rate is estimated to be $\sim 1.5 \times 10^5 [s^{-1}]$. On the other hand, the $E_r \times B$ shearing rate of $\sim 2.5 \times 10^5 [s^{-1}]$ produced by EIC at $r/a \sim 0.85$ is estimated experimentally from the above-mentioned profile of radial electric field. The estimated shearing rate is comparable or slightly larger than the growth rate predicted by GS2 code. This suppression of ITG mode might be attributed to the generation of significant sheared flow by EIC transiently.

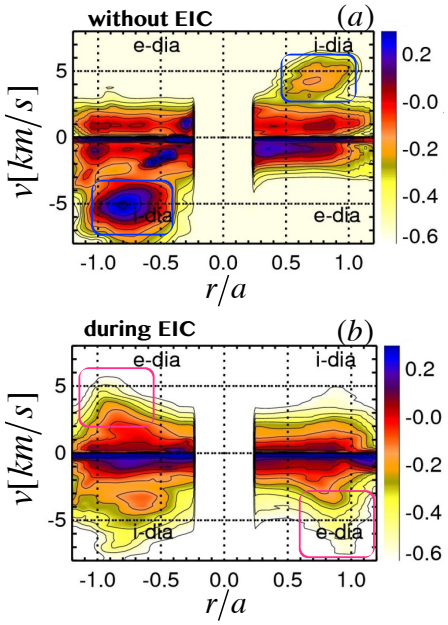

Fig. 7 The contour plots of the amplitude of density fluctuation as the function of the phase velocity and normalized minor radius without EIC (a) and during EIC (b).

In addition, the clear increase of carbon temperature is observed by CXRS during the suppression of the ITG like micro-turbulence, as shown in Fig. 6(c).

9. Summary

The resistive interchange modes destabilized through resonant interaction with a characteristic motion of helically trapped energetic ions are observed for the first time, exhibiting bursting character and rapid frequency chirping down, in the LHD plasmas. The initial frequency of the mode is consistently explained by the mode-particle resonance condition in an LHD plasma. This resonant interaction is clearly found in the rapid changes in the energy spectra of charge exchanged neutral flux measured by CNPA. The mode structures derived from ECE and SX diagnostics show that both EIC and RIC have quite similar eigenfunction of radial displacement. The eigenfunction is an even function around the mode rational surface and it indicates the interchange-type mode. The power scan of PERP-NBI suggests the existence of the threshold of beta value of helically trapped energetic ions to excite EIC. EIC strongly impacts on the confinement of helically trapped energetic ions. The non-ambipolar radial transport of helically trapped energetic ions is consistently inferred from the large and sudden drop of plasma potential measured by HIBP. Consistently, this radial electric field provides a large torque on the edge of plasma flow and forms a significant sheared flow, which contributes to clear suppression of micro-turbulence and improvement of bulk plasma confinement.

This work is in part supported by the NIFS budget (ULPP021 and ULPP028), the JSPS Grant-in-Aid for Scientific Research (B) 23340184 and 24360386, and the JSPS-NRF-NSFC A3 Foresight Program in the field of Plasma Physics

References

[1] M. Wakatani 1998 “Stellarator and Heliotron Devices” Oxford University Press
[2] K. Toi et al 2010 Fusion Sci. Technol. **58** 61
[3] K. Toi et al 2005 Phys. Plasmas **12** 020701
[4] K.Y. Watanabe et al 2010 Fusion Sci. Technol. **58** 160
[5] F. Watanabe et al 2007 Plasma and Fusion Res. **2** S1066
[6] F. Watanabe et al 2006 Plasma Phys. Control. Fusion **48** A201-A208
[7] K.Y. Watanabe et al 2011 Phys. Plasma **18** 056119
[8] A. Isayama et al 2006 Plasma Phys. Control. Fusion **48** L45
[9] B.A. Carreras et al 1987 Phys. Fluids **30** 1388
[10] R. Ueda et al 2014 Phys. Plasma **21** 052502
[11] S. Sakakibara et al 2008 Plasma Phys. Control. Fusion **50** 124014
[12] T. Watanabe et al 2006 Nucl. Fusion **46** 291
[13] K. Ida et al 2008 Rev. Sci. Instrum. **79** 053506
[14] M. Isobe et al 1999 Rev. Sci. Instrum. **70** 827
[15] Ya. I. Kolesnichenko et al 2002 Phys. Plasma **9** 2
[16] X.D. Du et al 2012 Plasma and Fusion Res. **7** 72401088
[17] K. Kawahata et al 2003 Rev. Sci. Instrum. **74** 1449
[18] S. Murakami et al 1995 Trans. Fusion Technol. **27** 259
[19] T. Ozaki et al 2000 Rev. Sci. Instrum. **71** 7
[20] M. Osakabe et al 2006 Nucl. Fusion **46** S911
[21] T. Ido et al 2006 Rev. Sci. Instrum. **77** 10F523
[22] N. Nakajima et al 1991 J. Phys. Soc. Japan **60** 12
[23] K.Y. Watanabe et al 1995 Nucl. Fusion **35** 335
[24] K. Tanaka et al 2008 Rev. Sci. Instrum. **79** 10E702
[25] W. Dorland et al 2000 Phys. Rev. Lett. **85** 5579
[26] D.R. Mikkelsen et al 2014 Phys. Plasma **21** 082302
[27] M.Nunami et al 2012 Phys. Plasma **19** 042504